

# Early Termination of Dyadic Region-Adaptive Hierarchical Transform for Efficient Attribute Compression of 3D Point Clouds

Reetu Hooda  and W. David Pan  , Senior Member, IEEE

**Abstract**—The low-complexity RAHT (Region-Adaptive Hierarchical Transform) and its corresponding Dyadic decomposition have been incorporated in the MPEG (Moving Picture Expert Group) standardization for encoding the attribute values in 3D point clouds. While significant gains were observed with the replacement of RAHT by Dyadic RAHT, the standard scheme uses only one type of decomposition for the entire point cloud. In this letter, we propose a novel adaptive scheme of switching between RAHT and Dyadic RAHT to achieve early termination of Dyadic RAHT by using 3D gradient filters. Improvements were made on the state-of-the-art scheme that uses only Dyadic RAHT transformation. The proposed method was tested on the publicly available 3D point cloud datasets. The results shows we can achieve cumulative compression gain of up to 11% over all-dyadic approach, by avoiding further decomposition in some cases.

**Index Terms**—Attribute compression, 3D sobel filter, Point clouds, RAHT, Dyadic RAHT.

## I. INTRODUCTION

A Point cloud (PC) is a collection of set of points in 3D space typically represented by geometric positions as 3D coordinates  $(x, y, z)$ . The coordinates can also have associated attribute values such as color information or normal vectors. Point cloud is a powerful 3D visual representations by providing a very realistic and interactive experience to the users [1], [2]. They provide multiple viewpoints and are extensively used in diverse applications such as autonomous driving, geographical information system and robotic applications etc. To efficiently represent the details entailing 3D scenes, an enormous amount of information is required. As the precision of the PC increases, the storage and the bandwidth requirements for transmission also increase [3]. Therefore, for practical usage of PC in aforementioned applications, efficient point cloud compression (PCC) techniques are of paramount importance.

The MPEG and JPEG community have initiated activities (MPEG call for proposal (CfP) in January 2017) related to the standardization of PCC [3], [4]. Due to PC's unstructured nature, the geometry and attribute information are generally encoded separately. The geometry is encoded using a popularly known Octree approach whereas, the attribute information can be encoded using a Haar-inspired transform called RAHT [5], [6], [7]. Several recent works have validated the effectiveness of dyadic decomposition-based methods but are used only in clinical applications such as detection of glaucoma [8] and diagnosis of COVID-19 [9]. There were some improvements reported by shifting from RAHT to Dyadic RAHT for attribute

encoding in PCs. Dyadic RAHT is a variation of RAHT which has been recently incorporated in the PCC standard [10], [11]. Dyadic RAHT transforms both low and high frequency components, thereby exploiting redundancies in both the sub-bands, whereas only low frequency components are transformed further in the case of RAHT [12], [13]. The existing standard has the limitation of using only one type of decomposition throughout the point cloud limiting the adaptability to its changing statistics which is resulting in reduced gains.

In this work, we propose to switch between these two variants of RAHT based on the characteristics of the blocks to be transformed. Early termination in Dyadic RAHT leads to a change in the BD-rate performance. The idea is to use Dyadic RAHT for denser and highly varying areas, while using RAHT for sparser & uniform areas in the point cloud. 3D Sobel operator-based edge detection is employed in order to identify the characteristics of the block to be transformed [14], [15], [16]. The proposed method is tested on publicly available datasets and compared to all-Dyadic RAHT approach, which is an improvement on all-RAHT scheme.

The rest of the letter is organized as follows: Section II provides detailed comparisons of the two types of decomposition used. Section III describes the switching scheme based on 3D edge detection. Section IV includes the simulation results and analysis of the BD-rate performance on the PC datasets. The letter is concluded in Section V.

## II. TYPES OF DECOMPOSITION

At first, three distinct techniques were defined by the MPEG group for the compression of different categories of PC data: Video-based PCC (V-PCC) for dynamic content, Surface PCC (S-PCC) for static surfaces, and Lidar PCC (L-PCC) for dynamically acquired LIDAR sequences. S-PCC and L-PCC shared some similarities due to which they were later merged together and referred to as Geometry-based PCC (G-PCC) [17]. In G-PCC, the geometry can be coded in a lossy manner by pruning the octree. For coding of attributes, one of the options in G-PCC is RAHT, which has been upgraded to Dyadic RAHT.

RAHT is a low-complexity hierarchical transform that is an extension of Haar transform in 3D domain. Let us consider a signal  $V$  containing  $N$  elements. At decomposition level  $l$ , two adjacent voxels  $V_{l+1,2n}$  and  $V_{l+1,2n+1}$  are transformed

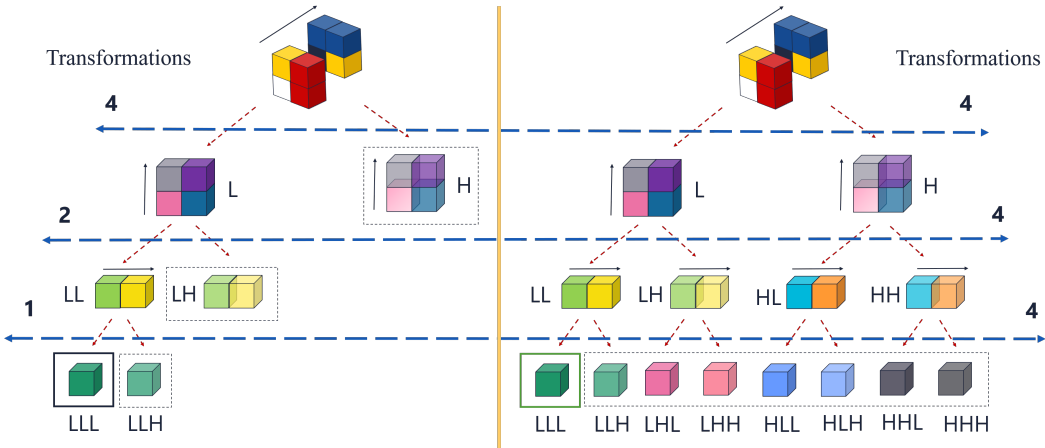


Fig. 1. RAHT (left) Versus Dyadic RAHT (right).

to generate low- and high-pass coefficients  $G_{l,n}$  and  $H_{l,n}$  as follows:

$$\begin{bmatrix} G_{l,n} \\ H_{l,n} \end{bmatrix} = \begin{bmatrix} \alpha & \beta \\ -\beta & \alpha \end{bmatrix} \begin{bmatrix} V_{l+1,2n} \\ V_{l+1,2n+1} \end{bmatrix} \quad (1)$$

where

$$\alpha = \sqrt{\frac{w_1}{w_1 + w_2}}, \quad \beta = \sqrt{\frac{w_2}{w_1 + w_2}}, \quad (2)$$

and  $w_1, w_2$  are the respective weights of the voxels  $V_{l+1,2n}$  and  $V_{l+1,2n+1}$ . Note that the transform is orthonormal, i.e.,  $\alpha^2 + \beta^2 = 1$ . The inverse transform is defined as follows:

$$\begin{bmatrix} V_{l+1,2n} \\ V_{l+1,2n+1} \end{bmatrix} = \begin{bmatrix} \alpha & -\beta \\ \beta & \alpha \end{bmatrix} \begin{bmatrix} G_{l,n} \\ H_{l,n} \end{bmatrix}. \quad (3)$$

In G-PCC, the RAHT decomposition is performed on  $2 \times 2 \times 2$  (=8) blocks in three steps. Since, two adjacent voxels are transformed at a time, the first step involves transforming 4 pairs of blocks to split the  $2 \times 2 \times 2$  blocks into low (L) and high (H) frequency components along the  $z$ -direction each of dimension  $2 \times 2 \times 1$ . Only the L sub-band is further transformed along the  $y$ -direction in step 2 to produce LL and LH (two pairs of blocks are processed) of dimension  $1 \times 2 \times 1$ . Finally, one pair of blocks are transformed to generate one DC coefficient (LLL) of dimension  $1 \times 1 \times 1$  and 7 AC coefficients highlighted in dashed box in Fig. 1. One operation of RAHT decomposition involves  $7 \times (4 + 2 + 1)$  transformations.

The dyadic RAHT decomposition is also performed on 8 blocks at a time, but now the high frequency components are also transformed further along the  $z, y$  and  $x$  directions, making a total of  $12 \times (4 + 4 + 4)$  transformations. A simplified illustration of the comparison between RAHT and Dyadic RAHT is shown in Fig. 1. The compression performance was improved by replacing RAHT with Dyadic RAHT decomposition, which helps by decorrelating the high frequency coefficients. Thus dyadic RAHT was incorporated in the standard compression scheme.

### III. 3D EDGE DETECTION

Let us consider a case where all the  $2 \times 2 \times 2$  blocks are occupied, whose attribute values are to be transformed. Although the dyadic decomposition can lead to better performance, the number of transformations will now increase to 12 when compared to RAHT, which requires only 7 transformations. Therefore, the complexity increases by a factor of  $12/7$  [10]. However, switching to dyadic decomposition will not lead to much increased complexity in lower occupancy cases.

To this end, we propose to study the characteristics of the neighbouring parent blocks in order to decide the type of decomposition needs to be employed in transforming the central block. The idea is to use RAHT for uniform areas and use dyadic decomposition for discontinuous region (which needs further breaking down of energy) in the point cloud. The goal is to improve the compression performance without much increased complexity. Now, let us consider a point or block at a certain level in the octree which is to be transformed, referred as central block and is surrounded by neighbouring blocks. The discontinuities in the central block shown in red in Fig. 2 are identified using its 18 neighbour parent blocks that share a face or an edge with the central block to be transformed [18]. We have considered 18-neighbourhood of the central block, since it covers more patterns with fewer masks [14], [19]. To adapt the decomposition to the characteristics of the PC, a 3D Sobel operator is utilized to determine the discontinuities in the central block. To evaluate the strength of the gradient  $G(x, y, z)$ , the proposed algorithm uses only the Luma component values of the 18 neighboring blocks for simplicity. The 3D Sobel operator is an orthogonal gradient operator. The gradient of a PC  $f$  at position  $(x, y, z)$  is defined in terms of directionally oriented spatial derivatives as:

$$\nabla f(x, y, z) = G(x, y, z) = [G_x G_y G_z]^T \quad (4)$$

where

$$\begin{aligned} G_x &= \frac{\partial f(x, y, z)}{\partial x} = S_x(x, y, z) * f(x, y, z), \\ G_y &= \frac{\partial f(x, y, z)}{\partial y} = S_y(x, y, z) * f(x, y, z), \\ G_z &= \frac{\partial f(x, y, z)}{\partial z} = S_z(x, y, z) * f(x, y, z), \end{aligned} \quad (5)$$

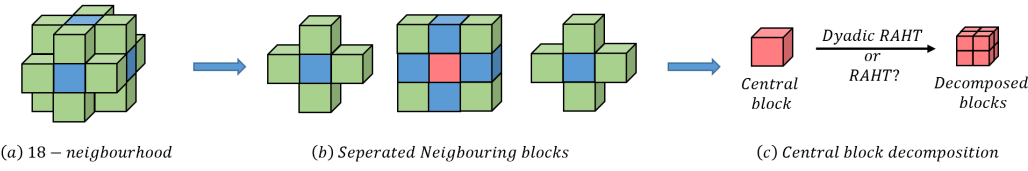


Fig. 2. Edge detection based on the neighbourhood.

are gradients in  $x, y$  and  $z$  direction, which point to the direction of the maximum rate of change in  $f$  at coordinate  $(x, y, z)$ . The operator uses the 3D Sobel edge kernels ( $S_x(x, y, z), S_y(x, y, z), S_z(x, y, z)$ ) (shown in Fig. 3) to perform the convolution (denoted by '\*' in Eq. (5)) in order to calculate the gradients  $G_x, G_y, G_z$ .

$$\begin{array}{ccc} \begin{array}{|c|c|c|} \hline -4 & & \\ \hline 0 & 0 & 0 \\ \hline 4 & & \\ \hline \end{array} & \begin{array}{|c|c|c|} \hline -4 & -8 & -4 \\ \hline 0 & 0 & 0 \\ \hline 4 & 8 & 4 \\ \hline \end{array} & \begin{array}{|c|c|c|} \hline -4 & & \\ \hline 0 & 0 & 0 \\ \hline 4 & & \\ \hline \end{array} \\ S_x(x, y, z) & & \\ \\ \begin{array}{|c|c|c|} \hline 0 & & \\ \hline -4 & 0 & 4 \\ \hline 0 & & \\ \hline \end{array} & \begin{array}{|c|c|c|} \hline 4 & 0 & 4 \\ \hline -8 & 0 & 8 \\ \hline -4 & 0 & -4 \\ \hline \end{array} & \begin{array}{|c|c|c|} \hline 0 & & \\ \hline -4 & 0 & 4 \\ \hline 0 & & \\ \hline \end{array} \\ S_y(x, y, z) & & \\ \\ \begin{array}{|c|c|c|} \hline -4 & & \\ \hline -4 & 0 & -4 \\ \hline 4 & & \\ \hline \end{array} & \begin{array}{|c|c|c|} \hline 0 & 0 & 0 \\ \hline 0 & 0 & 0 \\ \hline 0 & 0 & 0 \\ \hline \end{array} & \begin{array}{|c|c|c|} \hline 4 & & \\ \hline 4 & 0 & 4 \\ \hline 4 & & \\ \hline \end{array} \\ S_z(x, y, z) & & \end{array}$$

Fig. 3. Sobel template masks.

The magnitude of the gradient is calculated as:

$$mag(\nabla f) = \|\nabla f\| = \sqrt{G_x^2 + G_y^2 + G_z^2}. \quad (6)$$

For faster computation, the  $mag(\nabla f)$  can be approximated using absolute values defined as:

$$mag(\nabla f) \approx |G_x| + |G_y| + |G_z| \quad (7)$$

Then  $mag(\nabla f)$  is normalized using the average of the available blocks to find a ratio  $k$  (where  $0 \leq k \leq 1$ ) as:

$$k = \frac{mag(\nabla f)}{\text{average}}. \quad (8)$$

If  $k$  exceeds a certain threshold ( $T$ ), we then decide central block to be continuous region and is to be transformed using RAHT decomposition; otherwise dyadic is used.

The research idea stems from the intuition that RAHT decomposition will be more efficient for flat regions and dyadic decomposition for discontinuous region in the point cloud. To demonstrate that, we generated three solid cubical point clouds with non-uniform region and depth  $d = 4, 5$ , and  $6$  consisting of 4096, 32768 and 262144 points respectively and can be generalized as  $N \times N \times N$  where  $N = 2^d$ . A sample of one of the generated point clouds is shown

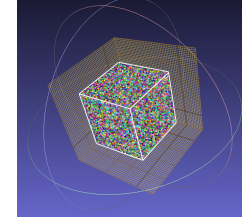


Fig. 4. Sample solid cube with depth = 5.

TABLE I  
CUMULATIVE GAINS OF DYADIC RAHT W.R.T RAHT FOR SAMPLE CUBES.

Depth	No. of Points	RAHT vs			
		T=0.2	T=0.4	T=0.6	T=0.8
4	4096	-0.7%	-1.8%	-2.2%	-3.7%
5	32768	-3.1%	-3.6%	-4.0%	-4.1%
6	262144	-3.7%	-4.5%	-4.6%	-4.7%

in Fig. 4. All-RAHT was considered as the baseline model for comparisons while we slowly start introducing dyadic decomposition by tuning the threshold ( $T$ ). When threshold is set to 0, it corresponds to All-RAHT and and threshold set to 1 corresponds to All-Dyadic. Table I shows the cumulative gain over three-channels as threshold increases. As expected, we observe improvements in gains as we move towards more and more of dyadic decomposition for the sample cubes, confirming that dyadic is efficient for such cubes which mostly comprises of regions full of edges. Therefore, based on the properties of a certain region in the PC, suitable decomposition is used to exploit the redundancies while saving on the number of transformation by avoiding dyadic in the case of uniform areas in the PC.

#### IV. EXPERIMENTAL RESULTS

To validate the efficiency of the proposed method, we tested our algorithm on three types of point cloud datasets. One LiDAR (overpass sequence), six static objects (Boxer, Egyptian mask, Loot, Red and black, Thai dancer and Basketball player) were chosen from the MPEG dataset [20] and frames extracted from dynamic sequences of MVUB (Microsoft Voxelized Upper Body [21]) dataset. The point cloud test set is illustrated in Fig. 5. The geometry and attributes were encoded in lossy manner. Since dyadic RAHT was an improvement on RAHT, we have compared the proposed algorithm to dyadic RAHT. To incorporate both bitrate and quality measurement, the evaluation was based on bitrate-distortion (BD) performance. The bitrate is calculated as the total number of bits in the

TABLE II  
BD-RATE GAINS AND APPROXIMATE RECORDED ENCODING-DECODING TIME (S) FOR PROPOSED SCHEME OVER DYADIC RAHT.

Test Sequences	No. of Points	BD-rate			All Dyadic		Proposed		Cumulative Gain			
		Luma	Cb	Cr	Enc	Dec	Enc	Dec	T=0.2	T=0.4	T=0.6	T=0.8
Boxer	3493085	2.7%	-6.0%	-5.7%	8.94	1.51	8.84	1.54	<b>-9.0%</b>	-4.5%	-2.8%	0.5%
EM (vox12)	272684	-0.9%	-5.0%	-3.5%	1.33	0.49	1.32	0.49	3.2%	-3.7%	<b>-9.4%</b>	-2.2%
Loot	3017285	0.3%	-0.4%	-1.0%	7.78	1.36	7.71	1.36	5.7%	3.1%	1.8%	<b>-1.1%</b>
Red and black	757691	-0.1%	-1.0%	0.1%	1.85	0.33	1.86	0.32	2.0%	1.1%	0.1%	<b>-1.0%</b>
Thai dancer	3130215	-1.2%	-0.5%	-0.9%	6.09	0.54	6.00	0.54	6.7%	4.7%	-1.7%	<b>-2.6%</b>
EM (vox20)	272689	0.1%	-2.9%	-2.5%	2.29	1.18	2.25	1.19	-1.8%	<b>-5.3%</b>	-4.7%	0.2%
Basketball player	2925514	3.1%	-9.2%	-4.9%	4.47	0.765	6.51	0.76	<b>-11.0%</b>	-10.5%	-1.5%	-4.7%
Andrew	279664	-0.7%	-9.0%	-1.1%	0.63	0.11	0.64	0.10	0.4%	-1.8%	-9.5%	<b>-10.8%</b>
Phil	370798	0.7%	-2.3%	-0.2%	0.86	0.14	0.86	0.14	6.6%	4.2%	<b>-1.8%</b>	-0.6%
Ricardo	960703	-1.0%	-0.6%	-2.6%	2.25	0.35	2.23	0.37	8.0%	3.9%	<b>-4.2%</b>	-2.2%
Sarah	302437	-0.9%	-1.2%	-2.3%	0.70	0.10	0.71	0.11	-1.4%	0.2%	-2.9%	<b>-4.4%</b>
overpass_q1mm	5255920	0.5%	-1.2%	-1.0%	50.01	13.79	68.40	19.93	<b>-1.7%</b>	-1.3%	-0.9%	-0.4%

bitstream by the total number of input points in PC, whereas the distortion is measured in terms of PSNR (peak signal to noise ratio) [1]. To make the comparison for wide range of bitrates, six point BD-rates were computed.



Fig. 5. Point cloud dataset (from left to right, top to bottom): Phil, Ricardo, Sarah, Andrew, Boxer, Red and black, Basketball player, Loot, Thai dancer, Egyptian mask, overpass.

The results comparing the proposed method and dyadic RAHT are summarized in Table II. A positive value of BD-rate corresponds to loss, whereas a negative value corresponds to PSNR gains at the same bitrate. After some tests and tuning, a threshold value of 0.2 (for Boxer, Basketball player and overpass), 0.4 (for Egyptian mask (vox20)), 0.6 (for Egyptian mask (vox12), Phil and Ricardo) and 0.8 for the remaining PC were used. From Table II, we observe that a maximum cumulative gain of 11% BD-rate gain was achieved with minimum cumulative gain of 1.7% in the worst case. In a majority of the datasets, BD-rate improvements can be observed. Therefore, the results demonstrate that it is advantageous to

switch between the two types of transform by determining the discontinuity in the central block using 3D edge detection, instead of using either only RAHT or dyadic RAHT.

*Computational Complexity:* The computational complexity of the proposed algorithm includes the computational cost of 3D edge detection, which is performed using convolution operation. Computation of 3D convolution for an image of dimension  $N \times M \times K$  with filter sizes of  $p \times q \times s$  is  $\mathcal{O}(NMKpq)$ , which can be further reduced to  $\mathcal{O}((N+p)(M+q)(K+s)\log((N+p)(M+q)(K+s)))$  using Fast Fourier Transform with some memory cost. We have used the direct implementation with an extreme case of 3493085 voxels convolved with  $p = q = s = 3$ , i.e.,  $3 \times 3 \times 3$  filter, which in turn is expected to have a nominal effect on the encoding and decoding time as validated by the approximate recorded time shown in Table II.

## V. CONCLUSION

We have introduced a new scheme that allows to switch between RAHT and Dyadic RAHT to adapt to the unordered nature of 3D point clouds. In order to effectively exploit the redundancies in uniform and non-uniform areas in a PC, the switch is based on the characteristics of the neighbourhood. The continuity and discontinuity are recognized by 3D edge detection using the Sobel operator. The experimental results on two different types of datasets show that the proposed algorithm achieves good BD-rate cumulative gains of up to 11% when compared to using only one type of transform throughout the point cloud without increasing the computational complexity. The limitation of the presented work lies in its threshold dependency which is currently tuned. In future, it would be of interest to use the tuned threshold values from the proposed technique in training a neural network to achieve generalized applicability and eliminating the threshold dependency.

## REFERENCES

- [1] A. F. R. Guarda, N. M. M. Rodrigues, and F. Pereira, "Point Cloud Coding: Adopting a Deep Learning-based Approach," in *2019 Picture Coding Symposium (PCS)*, 2019, pp. 1–5.
- [2] M. Quach, G. Valenzise, and F. Dufaux, "Learning Convolutional Transforms for Lossy Point Cloud Geometry Compression," *CoRR*, vol. abs/1903.08548, 2019. [Online]. Available: <http://arxiv.org/abs/1903.08548>
- [3] D. Graziosi, O. Nakagami, S. Kuma, A. Zaghetto, T. Suzuki, and A. Tabatabai, "An overview of ongoing point cloud compression standardization activities: video-based (V-PCC) and geometry-based (G-PCC)," *APSIPA Transactions on Signal and Information Processing*, vol. 9, p. e13, 2020.
- [4] P. Schelkens, T. Ebrahimi, A. Gilles, P. Gioia, K.-J. Oh, F. Pereira, C. Perra, and A. M. G. Pinheiro, "JPEG Pleno: Providing representation interoperability for holographic applications and devices," *ETRI Journal*, vol. 41, no. 1, pp. 93–108, 2019. [Online]. Available: <https://onlinelibrary.wiley.com/doi/abs/10.4218/etrij.2018-0509>
- [5] R. L. de Queiroz and P. A. Chou, "Compression of 3D Point Clouds Using a Region-Adaptive Hierarchical Transform," *IEEE Transactions on Image Processing*, vol. 25, no. 8, pp. 3947–3956, 2016.
- [6] E. Peixoto, "Intra-Frame Compression of Point Cloud Geometry Using Dyadic Decomposition," *IEEE Signal Processing Letters*, vol. 27, pp. 246–250, 2020.
- [7] G. P. Sandri, "Compression of Point Cloud Attributes," Ph.D. dissertation, University De Brasilia, Dec 2019.
- [8] P. K. Chaudhary and R. B. Pachori, "Automatic diagnosis of glaucoma using two-dimensional fourier-bessel series expansion based empirical wavelet transform," *Biomedical Signal Processing and Control*, vol. 64, p. 102237, 2021. [Online]. Available: <https://www.sciencedirect.com/science/article/pii/S1746809420303670>
- [9] P. K. Chaudhary and R. B. Pachori, "Automatic diagnosis of covid-19 and pneumonia using fbd method," in *2020 IEEE International Conference on Bioinformatics and Biomedicine (BIBM)*, 2020, pp. 2257–2263.
- [10] J. Taquet and S. Lasserre, "G-PCC On dyadic RAHT," *ISO/IEC JTC1/SC29/WG11 MPEG/m53557*, 2020.
- [11] D. R. Freitas, E. Peixoto, R. L. de Queiroz, and E. Medeiros, "Lossy Point Cloud Geometry Compression Via Dyadic Decomposition," in *2020 IEEE International Conference on Image Processing (ICIP)*, 2020, pp. 2731–2735.
- [12] S. Zhang, W. Zhang, F. Yang, and J. Huo, "A 3D Haar Wavelet Transform for Point Cloud Attribute Compression Based on Local Surface Analysis," in *2019 Picture Coding Symposium (PCS)*, 2019, pp. 1–5.
- [13] G. P. Sandri, P. A. Chou, M. Krivokuća, and R. L. de Queiroz, "Integer Alternative for the Region-Adaptive Hierarchical Transform," *IEEE Signal Processing Letters*, vol. 26, no. 9, pp. 1369–1372, 2019.
- [14] R. D. da Silva, R. Minghim, and H. Pedrini, "3D Edge Detection Based on Boolean Functions and Local Operators," *International Journal of Image and Graphics*, vol. 15, no. 01, p. 1550003, 2015. [Online]. Available: <https://doi.org/10.1142/S0219467815500035>
- [15] D. A. Hafiz, B. A. B. Youssef, W. M. Sheta, and H. A. Hassan, "Interest Point Detection in 3D Point Cloud Data Using 3D Sobel-Harris Operator," *International Journal of Pattern Recognition and Artificial Intelligence*, vol. 29, no. 07, p. 1555014, 2015. [Online]. Available: <https://doi.org/10.1142/S0218001415550149>
- [16] S. M. Ahmed, Y. Z. Tan, C. Chew, A. A. Mamun, and F. S. Wong, "Edge and Corner Detection for Unorganized 3D Point Clouds with Application to Robotic Welding," *CoRR*, vol. abs/1809.10468, 2018. [Online]. Available: <http://arxiv.org/abs/1809.10468>
- [17] S. Schwarz, M. Preda, V. Baroncini, M. Budagavi, P. Cesar, P. A. Chou, R. A. Cohen, M. Krivokuća, S. Lasserre, Z. Li, J. Llach, K. Mammou, R. Mekuria, O. Nakagami, E. Siahana, A. Tabatabai, A. M. Tourapis, and V. Zakharchenko, "Emerging MPEG Standards for Point Cloud Compression," *IEEE Journal on Emerging and Selected Topics in Circuits and Systems*, vol. 9, no. 1, pp. 133–148, 2019.
- [18] D. Flynn and S. Lasserre, "G-PCC CE13.18 report on upsampled transform domain prediction in RAHT," *ISO/IEC JTC1/SC29/WG11 MPEG/m49380*, July 2019.
- [19] D. Bazazian, J. R. Casas, and J. Ruiz-Hidalgo, "Fast and Robust Edge Extraction in Unorganized Point Clouds," in *2015 International Conference on Digital Image Computing: Techniques and Applications (DICTA)*, 2015, pp. 1–8.
- [20] E. d'Eon, B. Harrison, T. Myers, and P. A. Chou, "8i Voxelized Full Bodies – A Voxelized Point Cloud Dataset," *ISO/IEC JTC1/SC29/WG1 input document M74006* and *ISO/IEC JTC1/SC29/WG11 input document m40059*, Jan 2017. [Online]. Available: <http://plenodb.jpeg.org/pc/8ilabs/>
- [21] C. Loop, Q. Cai, S. O. Escalano, and P. A. Chou, "Microsoft Voxelized Upper Bodies – A Voxelized Point Cloud Dataset," *ISO/IEC JTC1/SC29 Joint WG11/WG1 (MPEG/JPEG) input document m38673/M72012*, May 2016. [Online]. Available: <http://plenodb.jpeg.org/pc/microsoft/>